3D Bioprinted Breast Cancer Model Reveals Stroma-Mediated Modulation of Extracellular Matrix and Radiosensitivity

Supplementary data

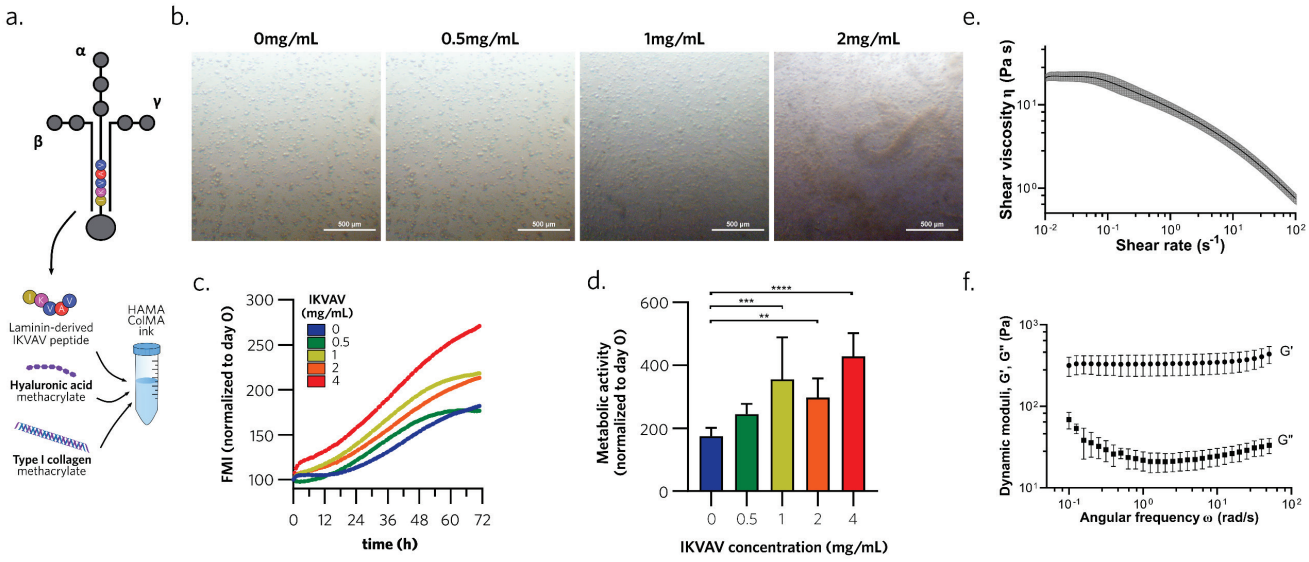

Supplementary Figure 1: IKVAV functionalized ink is mechanically suitable for bioprinting and supports MCF-7 growth.

a. Schematic representation of IKVAV peptide on laminin α chain, that is mixed with hyaluronic acid and collagen type I to compose the final hydrogel. **b.** Brightfield imaging of IKVAV functionalized HAMA-ColMA hydrogel at various concentrations of IKVAV peptide. Aggregates can be observed at 2mg/mL. Scale bars: 500µm. **c.** MCF-7 GFP+ fluorescence mean intensity (FMI) (N=3 n=6-11) for 72h post-seeding in the hydrogel at displayed concentrations. **d.** Metabolic activity at 7 days (right, N=3 n=5-12) after seeding in IKVAV functionalized hydrogel at the displayed concentrations. **e.** Viscometry of the HAMA-ColMA ink functionalized with 1mg/mL of IKVAV (N=3). **f.** Rheology of the HAM-ColMA + 1mg/mL IKVAV photopolymerized hydrogel (N=3). Shown is mean ± s.d. P values were computed with Kurskal Wallis test followed by Dunn's post hoc comparison test. **P<0.01;***P<0.001;****P<0.0001.

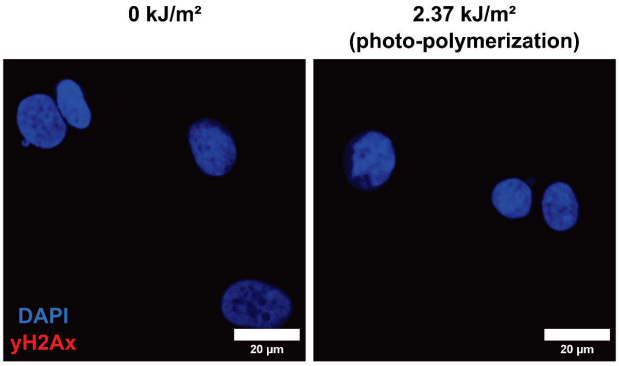

Supplementary Figure 2: DNA integrity is not disrupted by photo-polymerization.
Confocal images of MCF-7 cells stained for nucleus (DAPI, blue) and γH2Ax (red), irradiated to different doses. Scale bar: 20µm.

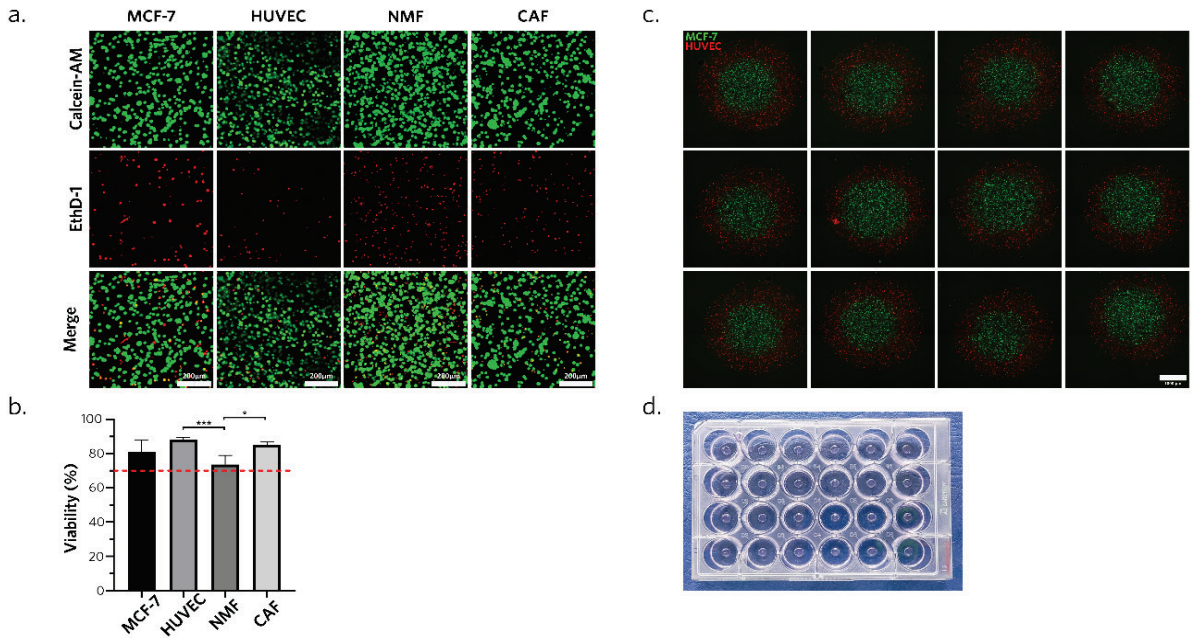

Supplementary Figure 3: BpBCM is obtainable reproducibly in a medium throughput fashion without altering cell viability.

a. Confocal images of the cell lines MCF-7, HUVEC, CAF and NMF bioprinted in the HAMA-ColMA-IKVAV hydrogel. Cells are stained with Calcein-AM (Live, green) and EthD-1 (Dead, red) 24h post-printing. Scale bars; 200µm. **b.** Viability quantification of the different cell lines 24h after microextrusion (N=3, n=5-13). The red dotted-line shows 70% viability limit from norm ISO-10993-5. **c.** Representative replicates of bioprinted models 4h post-printing. HUVEC mKate+ (red) were encapsulated in the stromal bioink and MCF-7 GFP+ (green) in the cancer bioink. Scale bar: 1000µm. **d.** Representative picture of a 24 well plate with models printed in the center of each well. Medium was removed from the wells for the picture. Shown are mean ± s.d. P values were computed by Kruskal-Wallis test followed by Dunn's post-hoc correction. *$p<0.05$; ***$p<0.001$.

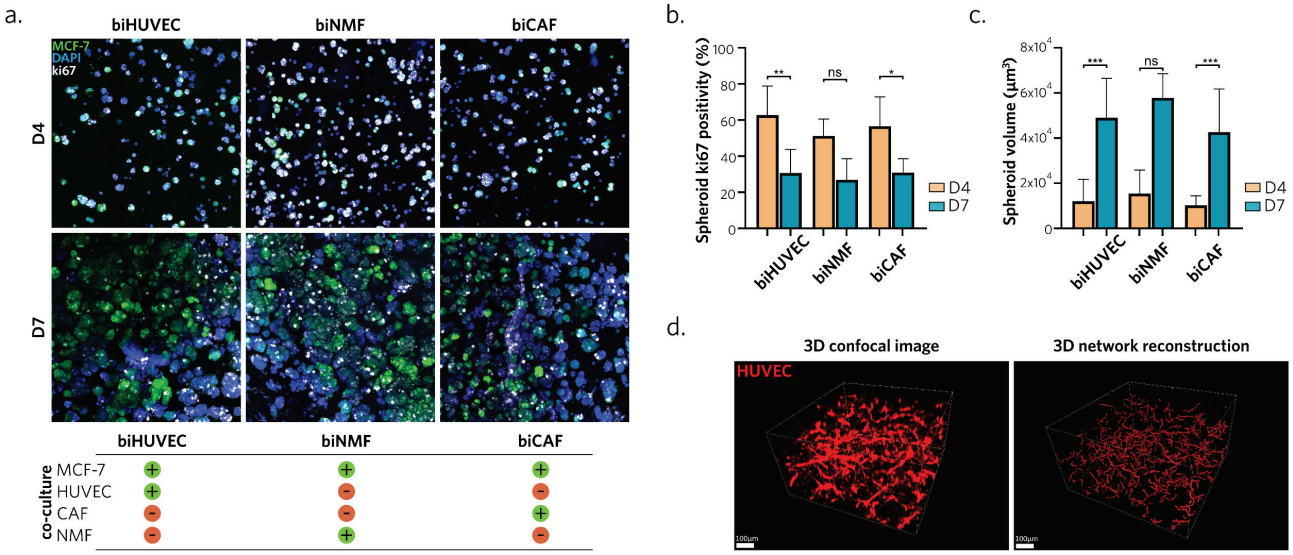

Supplementary Figure 4: bicultures with stromal cells does not affect cancer cell maturation and triCAF microvascular network develops in 3D

a. Representative ki67 immunostaining (gray), and stained nuclei using DAPI (blue), of BpBCM models printed with MCF-7 GFP+ (green) in co-culture conditions. Scale bar: 100µm. **b,c.** Spheroid volume (**b**) and ki67 spheroid positivity (**c**) on day 4 and 7 in the different culture conditions (N=3, n=4-12). **d**. Representative 3D image and microvascular network reconstruction from a triCAF condition HUVEC (red) confocal acquisition. Scale bars: 100µm. All data represent mean ± s.d. P-values were calculated with Kruskal-Wallis test corrected by Dunn's multiple comparison test. ns: non significant;*P<0.05;**P<0.01;***P<0.001.

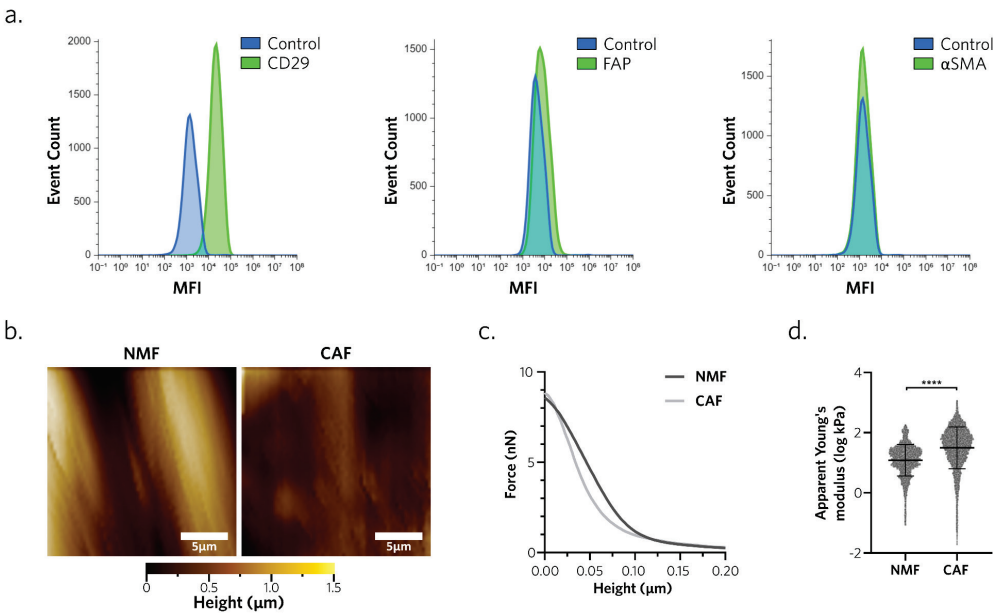

Supplementary Figure 5: Proteomics analysis of matrix deposition by CAF and NMF

a. Flow cytometry mean fluorescence intensity histogram of CAF cells stained for CD29, FAP and αSMA. Signal is compared to unstained cells as control. **b.** Topography images of atomic force microscopy experiment with similar surfaces. Scale bar: 5µm. **c**. Example force curve of CAF and NMF BpBCM. The steeper slope of CAF condition illustrates higher stiffness. **d.** Apparent Young's modulus distribution from individual curves measurement. Shown as mean ± s.d. P-values were calculated with Kruskal-Wallis test corrected by Dunn's multiple comparison test. ****p<0.0001.

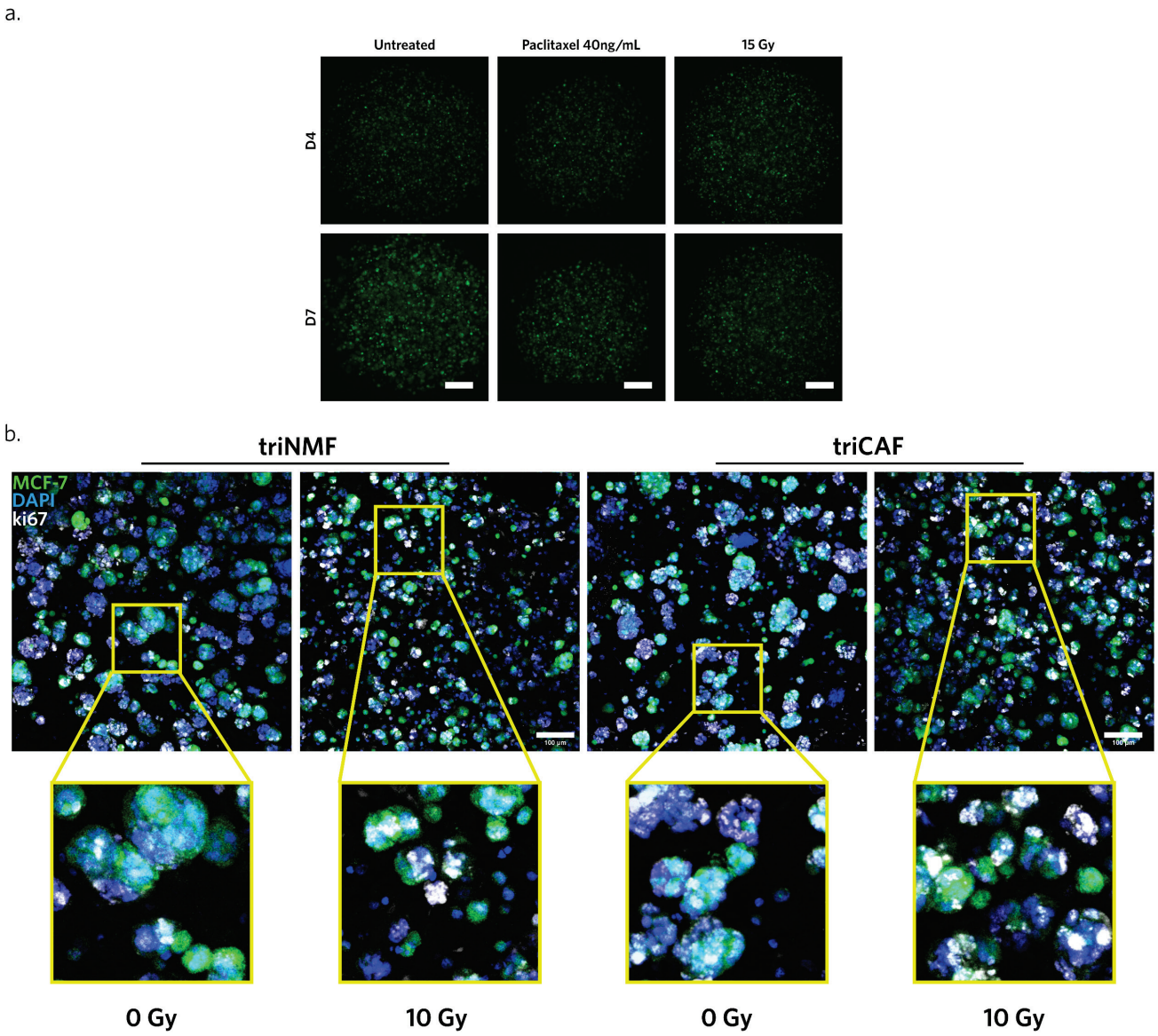

Supplementary Figure 6: Treated models imaging.

a. Representative acquisitions by epifluorescence of treated MCF-7 GFP+ (green) models used for quantifications in Fig.5b,c. Only control and maximum doses are displayed. Scale bar: 500µm. **b.** Full-size and close-up of Fig.5d. Representative immunostaining for ki67 (gray), MCF-7 GFP+ (green), nuclei (blue) of triNMF and triCAF models after 0 or 10 Gy irradiations. Scale bar: 100µm.

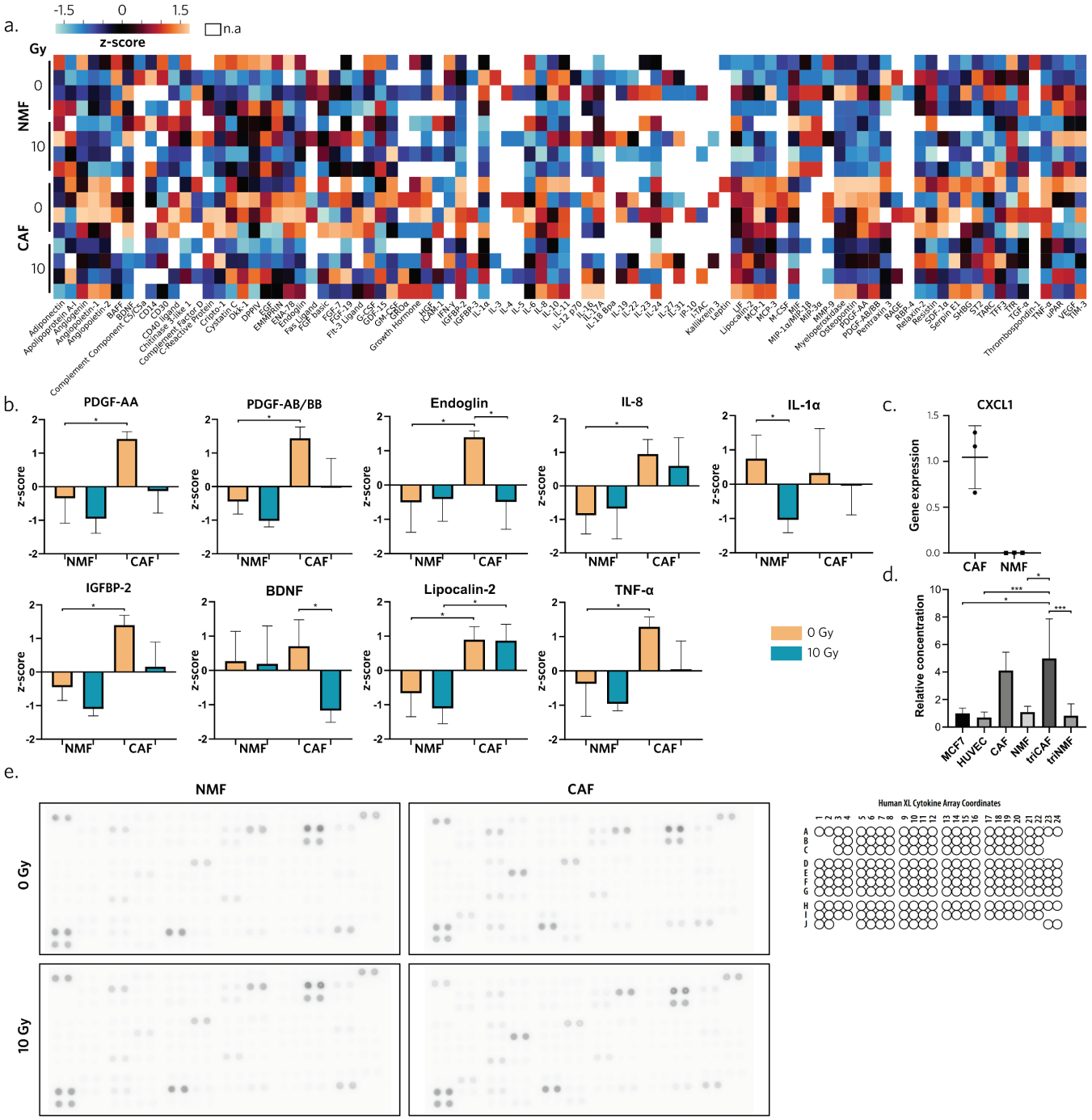

Supplementary Figure 7: Treatment and paracrine communication

a. Heatmap of the 91 detected cytokines in BpBCM medium conditioned for 72h post-treatment on day 4 (N=4). **b**. Representation of cytokines showing significant regulation between CAF and NMF, or after treatment. **c.** Relative mRNA expression of CXCL-1 in CAF or NMF cells (N=3). **d.** Relative CXCL-1 concentrations in BpBCM models in mono- or tricultures medium conditioned for 72h from day 4 to day 7 (N=3, n=2-10). **e.** Representative membranes chemiluminescence reading from the dot blot assays and grid coordinates. Protein

coordinates are available in appendix of Supplementary information. Shown as mean ± s.d. P-values were calculated with a 2-Way ANOVA corrected with Benjamini-Hochberg method (**b**) and Kruskal-Wallis test corrected by Dunn's multiple comparison test (**d**). *$p<0.05$; ***$p<0.001$.

Supplementary Video 1: Single model bioprinting

Video of the bioprinting process. The cancer center is deposited (slow motion) by a first printhead and pre-polymerized for 5s. A second printhead surrounds the center with the stromal periphery (slow motion) and the whole model is photo-polymerized for 30s.

Supplementary Video 2: Multimodel bioprinting

Video (speed x5) of the bioprinting process in a 24 well plate support. An additional printhead was used to dispense medium after each print.

Supplementary Video 3: MDA-MB-231 BpBCM invasion

3D reconstruction of a BpBCM printed with MDA-MB-231 breast cancer cell line (green) in the center cancer area instead of MCF-7. MDA-MB-231 cells are invading the stroma composed of fibroblasts and HUVEC (red) after 7 days. Scale bar: dynamic, visible on the video.

Supplementary Video 4: HRE-dUnaG model timelapse

Timelapse imaging of a BpBCM containing a cancer center with MCF-7 transduced with the HRE-dUnaG reporter (Green). The model was followed in brightfield (grey) and images were taken every 2h for 7 days. Scale bar: 1000µm.

Appendix

Dot blot protein coordinates.pdf

(from R&D Systems Proteome Profiler Human XL Cytokine Array manual ; Kit Catalog #: ARY022B)

APPENDIX

Refer to the table below for the Human XL Cytokine Array coordinates.

Coordinate	Analyte/Control	Entrez Gene ID	Alternate Nomenclature
A1, A2	Reference Spots	N/A	RS
A3, A4	Adiponectin	9370	Acrp30
A5, A6	Apolipoprotein A-I	335	ApoA1
A7, A8	Angiogenin	283	———
A9, A10	Angiopoietin-1	284	Ang-1, ANGPT1
A11, A12	Angiopoietin-2	285	Ang-2, ANGPT2
A13, A14	BAFF	10673	BLyS, TNFSF13B
A15, A16	BDNF	627	Brain-derived Neurotrophic Factor
A17, A18	Complement Component C5/C5a	727	C5/C5a
A19, A20	CD14	929	———
A21, A22	CD30	943	TNFRSF8
A23, A24	Reference Spots	N/A	RS
B3, B4	CD40 ligand	959	CD40L, TNFSF5, CD154, TRAP
B5, B6	Chitinase 3-like 1	1116	CHI3L1, YKL-40
B7, B8	Complement Factor D	1675	Adipsin, CFD
B9, B10	C-Reactive Protein	1401	CRP
B11, B12	Cripto-1	6997	Teratocarcinoma-derived Growth Factor
B13, B14	Cystatin C	1471	CST3, ARMD11
B15, B16	Dkk-1	22943	Dickkopf-1
B17, B18	DPPIV	1803	CD26, DPP4, Dipeptidyl-peptidase IV
B19, B20	EGF	1950	Epidermal Growth Factor
B21, B22	EMMPRIN	682	CD147, Basigin
C3, C4	ENA-78	6374	CXCL5
C5, C6	Endoglin	2022	CD105, ENG
C7, C8	Fas Ligand	356	TNFSF6, CD178, CD95L
C9, C10	FGF basic	2247	FGF-2
C11, C12	FGF-7	2252	KGF
C13, C14	FGF-19	9965	———
C15, C16	Flt-3 Ligand	2323	FLT3LG
C17, C18	G-CSF	1440	CSF3
C19, C20	GDF-15	9518	MIC-1
C21, C22	GM-CSF	1437	CSF2
D1, D2	GROα	2919	CXCL1, MSGA-α
D3, D4	Growth Hormone	2688	GH, Somatotropin
D5, D6	HGF	3082	Scatter Factor, SF
D7, D8	ICAM-1	3383	CD54
D9, D10	IFN-γ	3458	IFNG
D11, D12	IGFBP-2	3485	———

APPENDIX *CONTINUED*

Coordinate	Analyte/Control	Entrez Gene ID	Alternate Nomenclature
D13, D14	IGFBP-3	3486	————
D15, D16	IL-1α	3552	IL-1F1
D17, D18	IL-1β	3553	IL-1F2
D19, D20	IL-1ra	3557	IL-1F3
D21, D22	IL-2	3558	————
D23, D24	IL-3	3562	————
E1, E2	IL-4	3565	————
E3, E4	IL-5	3567	————
E5, E6	IL-6	3569	————
E7, E8	IL-8	3576	CXCL8
E9, E10	IL-10	3586	————
E11, E12	IL-11	3589	————
E13, E14	IL-12 p70	3593	————
E15, E16	IL-13	3596	————
E17, E18	IL-15	3600	————
E19, E20	IL-16	3603	————
E21, E22	IL-17A	3605	IL-17, CTLA8
E23, E24	IL-18 Bpa	10068	————
F1, F2	IL-19	29949	————
F3, F4	IL-22	50616	IL-TIF
F5, F6	IL-23	51561	IL-23A, SGRF
F7, F8	IL-24	11009	C49A, FISP, MDA-7, MOB-5, ST16
F9, F10	IL-27	246778	————
F11, F12	IL-31	386653	————
F13, F14	IL-32	9235	————
F15, F16	IL-33	90865	C9orf26, DVS27, NF-HEV
F17, F18	IL-34	146433	C16orf77
F19, F20	IP-10	3627	CXCL10
F21, F22	I-TAC	6373	CXCL11, SCYB9B
F23, F24	Kallikrein 3	354	PSA, KLK3
G1, G2	Leptin	3952	OB
G3, G4	LIF	3976	————
G5, G6	Lipocalin-2	3934	NGAL, LCN2, Siderocalin
G7, G8	MCP-1	6347	CCL2, MCAF
G9, G10	MCP-3	6354	CCL7, MARC
G11, G12	M-CSF	1435	CSF1
G13, G14	MIF	4282	————
G15, G16	MIG	4283	CXCL9

APPENDIX *CONTINUED*

Coordinate	Analyte/Control	Entrez Gene ID	Alternate Nomenclature
G17, G18	MIP-1α/MIP-1β	6348/6351	CCL3/CCL4
G19, G20	MIP-3α	6364	CCL20, Exodus-1, LARC
G21, G22	MIP-3β	6363	CCL19, ELC
G23, G24	MMP-9	4318	CLG4B, Gelatinase B
H1, H2	Myeloperoxidase	4353	MPO, Lactoperoxidase
H3, H4	Osteopontin	6696	OPN
H5, H6	PDGF-AA	5154	————
H7, H8	PDGF-AB/BB	5154/5155	————
H9, H10	Pentraxin 3	5806	PTX3, TSG-14
H11, H12	PF4	5196	CXCL4
H13, H14	RAGE	177	————
H15, H16	RANTES	6352	CCL5
H17, H18	RBP-4	5950	————
H19, H20	Relaxin-2	6019	RLN2, RLXH2
H21, H22	Resistin	56729	ADSF, FIZZ3, RETN
H23, H24	SDF-1α	6387	CXCL12, PBSF
I1, I2	Serpin E1	5054	PAI-I, PAI-1, Nexin
I3, I4	SHBG	6462	ABP
I5, I6	ST2	9173	IL-1 R4, IL1RL1, ST2L
I7, I8	TARC	6361	CCL17
I9, I10	TFF3	7033	ITF, TFI
I11, I12	TfR	7037	CD71, TFR1, TFRC, TRFR
I13, I14	TGF-α	7039	TGFA
I15, I16	Thrombospondin-1	7057	THBS1, TSP-1
I17, I18	TNF-α	7124	TNFSF1A
I19, I20	uPAR	5329	PLAUR
I21, I22	VEGF	7422	BEGFA
J1, J2	Reference Spots	N/A	RS
J5, J6	Vitamin D BP	2638	VDB, DBP, VDBP
J7, J8	CD31	5175	PECAM-1
J9, J10	TIM-3	84868	HAVCR2
J11, J12	VCAM-1	7412	CD106
J23, J24	Negative Controls	N/A	Control (-)